




Article

Dual-band Monopole Antenna Integrated with Frequency Selective Surface for Possible Use in Non-invasive Biomedical Applications

Isaú de Sousa Silva Junior¹, Alfredo Gomes Neto², Maurício Weber Benjô da Silva³

Antonio Luiz Pereira de Siqueira Campos¹

¹Communication Engineering Department, Federal University of Rio Grande do Norte, Natal, RN, Brazil,
isaujr.hiago@gmail.com, antonio.campos@ufrn.br

²Federal Institute of Education, Science and Technology of Paraíba, João Pessoa, PB, Brazil,
alfredogomesjpa@gmail.com

³Telecommunications Engineering Department, Fluminense Federal University, Niterói, RJ, Brazil,
mauriciobenjo@id.uff.br

Abstract— This work proposes the integration of a monopole antenna with a frequency selective surface (FSS) with double square loop geometry, which operates in the ISM (2.4 – 2.4835 GHz) and IEEE 802.11 WLAN (5.15–5.725 GHz) bands. The FSS was developed to be integrated into a microstrip monopole antenna, aiming to improve some of its radiative features, such as gain, directivity, and front-to-back ratio (FBR). We show that the double square loop FSS operates in bands from 1.91 to 3 GHz and from 4.64 to 6.56 GHz, fully covering the bands of interest. A prototype of the proposed structure was assembled and both the numerical simulation and the experimental results show that the antenna integrated with FSS presents significant improvements in all parameters, compared to the antenna without FSS. Because of the interest frequency ranges the proposed structure can be applied in non-invasive biomedical applications.

Index Terms— Dual-band Antenna, Frequency Selective Surface, Monopole antenna, Non-invasive Biomedical Applications

I. INTRODUCTION

Microstrip antennas have been the subject of intense research around the world due to the inherent qualities of this kind of antenna, such as lightness, low profile, low production cost, and aerodynamic profile [1]. These types of antenna have been implemented for some time in military applications, such as aircraft, satellites, and even high-performance missiles [2]. In addition, there are currently several other government and commercial applications that use this type of antenna, such as radio frequency identification systems (RFID) technology and energy harvesting systems, to name a few [3], [4].

Due to the several advantages, there was a growing development of research in the use of microstrip antennas in non-contact sensors for different applications, among which we can mention biomedical applications [5], [6]. However, it is known that microstrip antennas have some undesirable features, which may limit their applications: low directivity, low efficiency and they are, inherently, narrowband devices.

One of the ways to mitigate the disadvantages of the microstrip antenna is to integrate it with an FSS [7], [8], which can be inserted as a reflector on the back of the antenna, to reflect most of the

power radiated in its direction to the opposite direction, thus reinforcing the power radiated to the front of the antenna, improving antenna gain, directivity and front-to-back ratio [9].

On the other hand, the rapid development of wireless communication technology, invasive (implanted in the human body) and non-invasive (positioned above human tissue) biomedical sensor technology has gained a lot of space, resulting in a widely growing field of body-centric wireless networks (BCWNs). In-body, on-body, and off-body are different forms of body-centric wireless networks. On-body communication references wearable devices and non-invasive biomedical sensors. Communication between an on-body device and an external device is referred to in the literature as off-body communication. Finally, in-body communication involves communication between an implantable device and an external device for monitoring health parameters [10], [11].

Off-body communication is a key aspect of non-invasive biomedical sensor technology, as it is responsible for the connection between sensors and external devices. Therefore, the antennas used for this connection are extremely important and must meet specific electromagnetic requirements such as wide bandwidth, good gain levels, high efficiency, unidirectional radiation diagram (broadside direction), and consequently good front-to-back ratio [12]. Furthermore, characteristics such as lightness, small size, and low manufacturing cost are also important requirements for these antennas.

Thus, this work is an extended version of [13], and it proposes the integration of a dual-band microstrip monopole planar antenna with an FSS-based reflector, aiming at non-invasive biomedical applications. Through the two resonances generated by the FSS responses with a double square loop, we can improve the radiative features of the monopole antenna. Finally, a sample of the proposed structure is fabricated and measured to validate the simulation results.

This work consists of four sections: In addition to this introductory section, Section 2 presents a survey of the most recent literature related to the topic of the proposed framework. Section 3 presents the design, analysis and simulation results of the reflector and the antenna integrated with the reflector, Section 4 shows the results of the developed prototype and, finally, Section 5 concludes the work.

II. STATE OF THE ART

In [11], a compact tri-band adhesive planar antenna was proposed to operate as a gateway for biomedical applications, operating in the ISM band (2.4–2.5 GHz), in the WBAN UWB (3.1–10.6 GHz) and in the WLAN band (5.15–5.725 GHz). The antenna can be useful in body-signal monitoring and exhibits omnidirectional fields.

In [14], a design of a miniaturized and efficient dual-band antenna integrated with a metamaterial superstrate is presented. The antenna operates at ISM and WBAN bands. The total size was $50 \times 50 \times 1.6 \text{ mm}^3$. An enhancement in bandwidth, gain, and directivity was observed. The structure presents a low profile, higher gain, and low SAR.

In [15], a wearable dual-band folded-ring antenna, with directional radiation pattern, high-gain, high-efficiency, and low-specific absorption rate (SAR) performance, is presented, for operation in dual-band configuration at ISM and 5G 3.5 GHz bands. The proposed antenna can be applied in off-body communication. It is comprised of two substrates: a folded-ring antenna as a main radiator is printed on a low-loss rigid substrate and a conductive textile is attached to a felt substrate. The conductive textile is used as the ground plane and as a protective shield to prevent incidental electromagnetic waves from propagating toward the human body. The felt substrate provides a comfortable surface for wearers.

In [16], a dual-band antenna was designed to realize multiple functions in biomedical communications. Based on microstrip antenna, slots and slow-wave structure are adopted, lowering frequency. Via loading shorting pins, different operating modes are excited. The proposed antenna operates at 915 MHz for omnidirectional in-body communication and at 2.45 GHz for circularly polarized off-body radiation. The proposed antenna has different radiated characteristics in different bands, which can realize multifunctions in biomedical communications.

In [17], a miniaturized Ka/V dual-band mmWave microstrip antenna for 5G BCN (Body communication network) applications. The antenna has very small dimensions of $2.28 \times 3.06 \times 0.14 \text{ mm}^3$ and operates at Ka and V bands. The performance of the antenna is examined for off-body, on-body, and in-body BCN application scenarios. The antenna performs quite well at all interested frequencies. The antenna is suitable for most of the commercial next-generation BCN applications like the Internet of Healthcare, environment monitoring, and entertainment.

In [18], a tri-band hexagonal-shaped patch antenna for application in body area networks as well as healthcare communication is proposed. It satisfies the ISM band for on/off body communications. The antenna resonates at the 2.5 GHz, 5.5 GHz, and 10 GHz bands with gains of 5.175 dB, 8.28 dB, and 13 dB respectively. The antenna supports a high data rate off-body in the bands specified for wearable devices.

In [19], an Ashoka tree-shaped wearable textile antenna for biomedical and military applications working at 2.4 GHz and 9.04 GHz is investigated and analyzed. The designed antenna has a size of $34 \times 40 \times 1 \text{ mm}^3$. A textile material is employed as a non-conductive dielectric substance to define wearable applications. Simulation results are carried out under various bending conditions, both in free space and close to the human body. The suggested antenna performs satisfactorily in terms of gain and specific absorption rate. The suggested antenna is a solid contender for wearable applications that are both off- and on-body. Due to its characteristics, this antenna can be significantly used in military jackets and in biomedical applications.

In [20], another textile antenna integrated with metasurface is proposed. The proposed antenna has a low profile and its performance was investigated in free space and on a human body. Incorporating a metasurface structure on the antenna, the gain was improved from 6.1 dBi to 9.08 dBi. The antenna operates in a bandwidth ranging from 6 to 12 GHz, which is preferred for WBAN applications. The antenna displayed a Front-to-Back Ratio (FBR) of approximately 15 dB, which is essential for WBAN to avoid back radiation from the body. The developed structure could assist in the fabrication of unique WBANs and healthcare monitoring devices.

In [21], a hybrid Tri-band dielectric resonator antenna (DRA) for biomedical applications is proposed. The resulting structure is fed via a microstrip feed line. A rectangular dielectric resonator antenna with a rectangular patch with a cross-shaped slot is designed to exhibit a tri-band. The suggested antenna could be operated over two ISM bands (2.45/5.8GHz) and WiMAX (3.8 GHz). The proposed antenna performance is analyzed with body interaction as well as free space and is quite suitable for WBAN application. According to external analysis of the antenna, it could be especially suitable for biomedical applications.

In [22], the proposed antenna follows the line of flexible substrate. A wideband low-profile radiating G-shaped strip is proposed to operate as biomedical antenna for off-body communication. The antenna is designed to produce circular polarization over the frequency range 5 – 6 GHz to communicate with

WiMAX/WLAN antennas and it is designed to produce linear polarization over the frequency range 6 – 19 GHz for communication with the on-body biosensor antennas. To be fabricated on only one face of the flexible dielectric substrate, the antenna is fed through a co-planar waveguide (CPW). The proposed antenna covers the 5GHz frequency band of the WiMAX/WLAN applications within its 3dB-AR frequency band. The overall antenna dimensions are $25 \times 27 \times 0.13 \text{ mm}^3$.

In [23], a novel design of a miniaturized dual-band antenna for ISM implantable applications working at 915 MHz and 2.4 GHz was proposed. The antenna has a compact size of $6 \times 6 \times 0.25 \text{ mm}^3$ and shows a wide bandwidth of 12.6% and 12.8% and gain values of -21.8 dBi and -19.2 dBi at 915 MHz and 2.4 GHz, respectively.

A dual-band microstrip antenna with a circular and rectangular patch designed on textile material as substrate is proposed in [24] for military and biomedical applications, with a total size of $80 \times 80 \times 2 \text{ mm}^3$. To achieve dual-band operation slots were loaded into the patch. As a result, the proposed antenna presented improved radiative parameters in both operating bands.

In [25], the integration of an antenna with metasurfaces is proposed to improve radiation performance in the vicinity of the human body in biomedical applications. To this end, the authors incorporate two metasurface layers, the first that acts as an impedance matching layer between the radiating element and the biological tissue and the second that acts as an artificial magnetic conductor (AMC) as a support element for the antenna, to improve gain and reduce unwanted counter radiation. Numerical and experimental results demonstrated improved performance of the antenna operating at 2.56 GHz in terms of tissue field penetration and better radiation behavior.

An oval-shaped flexible monopole antenna operating at 2.45 GHz and backed by an electromagnetic bandgap array is proposed in [26]. By incorporating the EBG array as an isolator, greater antenna proximity to the human body and gain improvements in free space and in the vicinity of the human body were achieved. The antenna has dimensions of $59 \times 55 \times 0.1 \text{ mm}^3$ and can be used in WBAN and medical/sporting applications.

In [27], the authors propose an ultra-wideband (UWB) antenna for medical microwave imaging (MWI) applications operating in the 1–6 GHz frequency band. A UWB balun was attached to the flat arms of the bow tie providing high efficiency very low radiation and reverse radiation, which also caused an increase in the total size of the antenna ($60 \times 60 \times 50 \text{ mm}^3$).

As a novelty, this work presents a structure with very simple geometries, easy to manufacture and with high gain in both operating bands, obtained using the FSS reflector. Furthermore, the proposed antenna can be used for base stations of remote patient monitoring systems, as it can operate in two unlicensed frequency bands.

III. DESIGN AND ANALYSIS

In this section, we will present the optimization of the physical dimensions of the FSS and the antenna. Two subsections will present a parametric analysis to obtain optimized results.

A. FSS Analysis

The project began with designing a frequency-selective surface integrated with a microstrip monopole with two operating bands. The idea is to modify the antenna's radiation diagram, transforming it from omnidirectional to unidirectional, to continuously improve the antenna's front-to-back ratio, gain,

and directivity. This will make the antenna's operational characteristics more suitable for off-body communication in biomedical applications.

The first step is to choose the geometry of the unit cell, which best suits the purpose of the project. The chosen geometry was the double square loop, as this geometry presents a double-band response, good angular stability, and polarization independence [28].

After choosing the geometry, it was established that the substrate used would be FR4 ($\epsilon_r = 4.4$ and $\tan\delta = 0.02$), and then the initial dimensions, illustrated in Fig. 1 of the double square loop were calculated. The calculation of the initial dimensions was done using the following methodology, initially, the effective dielectric permittivity was calculated, as an average between the permittivity of the substrate and the permittivity of the air. Thus, obtaining an effective permittivity of 2.7. Then, the value of ϵ_r found was used to calculate the guided wavelength $\lambda_g = c/(f_r\sqrt{\epsilon_{eff}})$ with the resonance frequency of the desired operating band, that is, for the frequencies of 2.5 GHz and 5.5 GHz. Thus, the calculated wavelengths were 73.03 mm, for 2.5 GHz, and 33.20 mm, for 5.5 GHz.

Thus, the initial physical dimensions of the square loops were calculated so that the side of the outer square loop corresponds to $\lambda_g/4$ of the wavelength calculated for the 2.5 GHz frequency, while the length of the inner square loop was calculated as being $\lambda_g/4$ of the wavelength calculated for 5.5 GHz. This way, $L_{out} = 18.30$ mm and $L_{in} = 8.30$ mm are obtained because 0.3 mm is the smallest dimension we can manufacture. The loops' width was defined as 1 mm by design choice. Other design choices made initially were a substrate thickness of 1.6 mm and a unit cell period of 19.30 mm. The physical dimensions of the unit cell are illustrated in Fig.1 and its dimensions are listed in Table I.

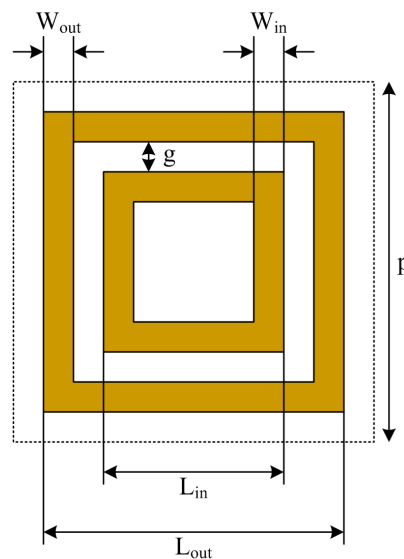


Fig. 1. Proposed FSS unit cell.

The designed FSS was simulated and the results showed that it did not present a second operating band within the desired frequency spectrum. However, the ISM operating band presents a behavior very close to that expected, with a resonance frequency of 2.4 GHz and a bandwidth of 1 GHz. To adapt the frequency response of the FSS to what is desired, the structure was subjected to a process of optimizing the physical dimensions, so that each dimension of the structure was subjected to a process of parametric analysis carried out in the Ansys HFSS software.

The FSS optimization process was started as Lin's parametric analysis. The result of this analysis is

TABLE I. INITIAL DIMENSIONS OF THE DESIGNED FSS.

Parameter	Dimension (mm)
L_{out}	18.30
L_{in}	8.30
W_{out}	1
W_{in}	1
P	19.30
h	1.6

illustrated in Fig. 2 and it can be seen that the increase in L_{in} results in a reduction in the resonance frequency of the second operating band, while the resonance frequency of the first operating band remains unchanged, occurring only the decrease in bandwidth.

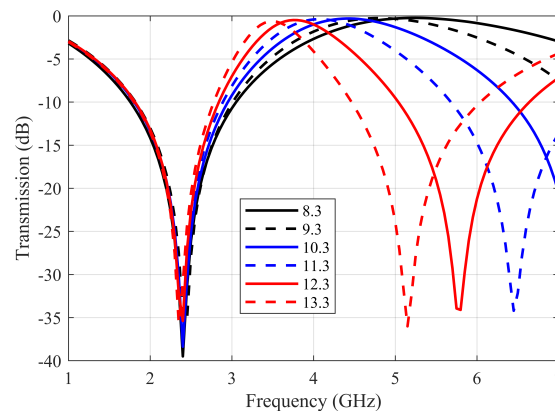


Fig. 2. Frequency response of the FSS for different values of L_{in} .

Similarly, the L_{out} dimension was also subjected to a parametric analysis, to observe the effects of this variation on the frequency response of the structure. The S_{21} obtained for this simulation, with different L_{out} values, can be seen in Fig. 3. It is possible to notice that the increase in L_{out} produces a reduction in the resonance frequency of the first operating band, while the resonance frequency of the second band remains unchanged. Increasing dimensions L_{in} and L_{out} increases the inductance and capacitance of the array, respectively, which justifies the reduction in the resonance frequencies of the corresponding bands.

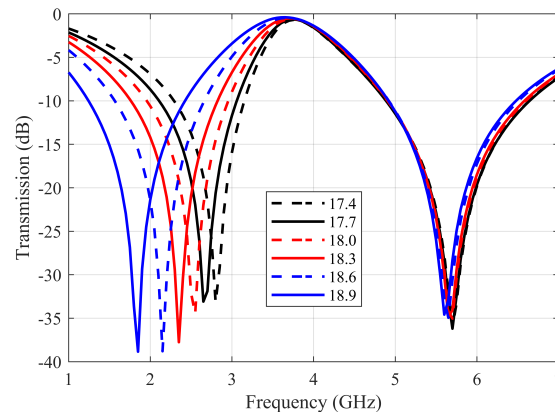


Fig. 3. Frequency response of the FSS for different values of L_{out} .

Another optimized parameter of the FSS was the width of the tapes of the square loops, W_{in} and W_{out} . Analyzing Fig. 4, it is possible to see that the variation of W_{in} affects significantly only the second resonance frequency, while the first resonance frequency appears insensitive to such variation. The second resonance frequency increases significantly with increasing W_{in} , which shows that the inductance of the smaller loop decreases with increasing W_{in} .

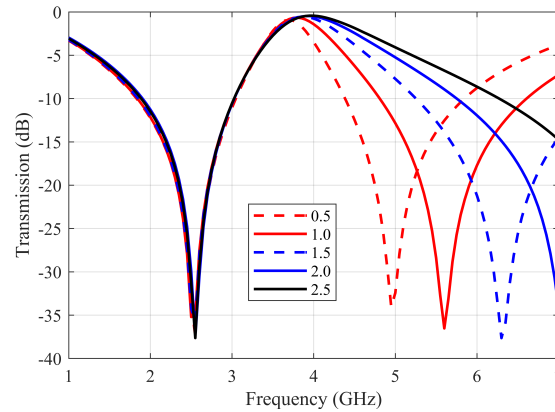


Fig. 4. Frequency response of the FSS for different values of W_{in} .

From Fig. 5, it can be seen that the first resonance frequency is affected by the variation of W_{out} , increasing with the increase of W_{out} . This increase in resonant frequency is due to the decrease in the inductance of the array. The second resonance frequency changes less, because this dimension increases a capacitance, but less than increases inductance.

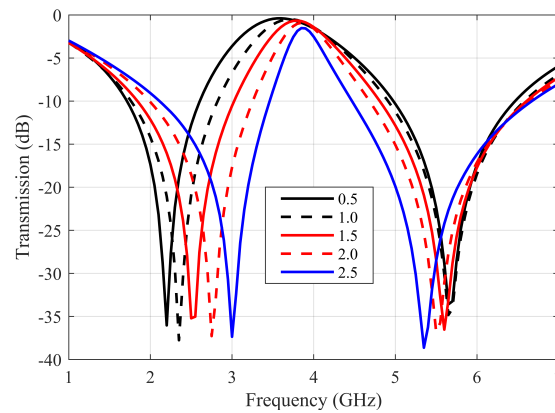


Fig. 5. Frequency response of the FSS for different values of W_{out} .

Finally, the behavior of S_{21} of the structure was also investigated for different values of the periodicity, P . The results of this investigation can be seen in Fig. 6, in which it is verified that the increase in P increases the two resonance frequencies but the second resonance is little affected, one since it reduces the capacitances of the array, for the first resonance and almost unchanged the second resonance.

From the parametric analysis developed, it was possible to define the optimal values of the physical dimensions of the designed FSS unit cell, all plotted in red continuous line. The optimized values are listed in Table II. These final values were chosen so that the FSS presented two operating bands covering the 2 to 3 GHz and 5 to 6 GHz bands. As the FSS will function as a reflector, it must present a linear phase in the bands of interest. The module and phase of S_{21} are illustrated in Fig. 7. It can be seen that the requirements have been met, for the optimized FSS.

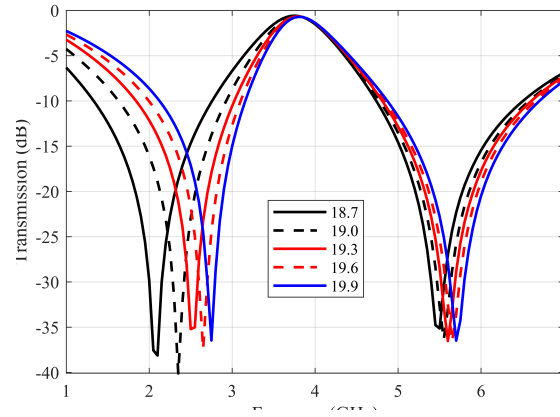


Fig. 6. Frequency response of the FSS for different values of P .

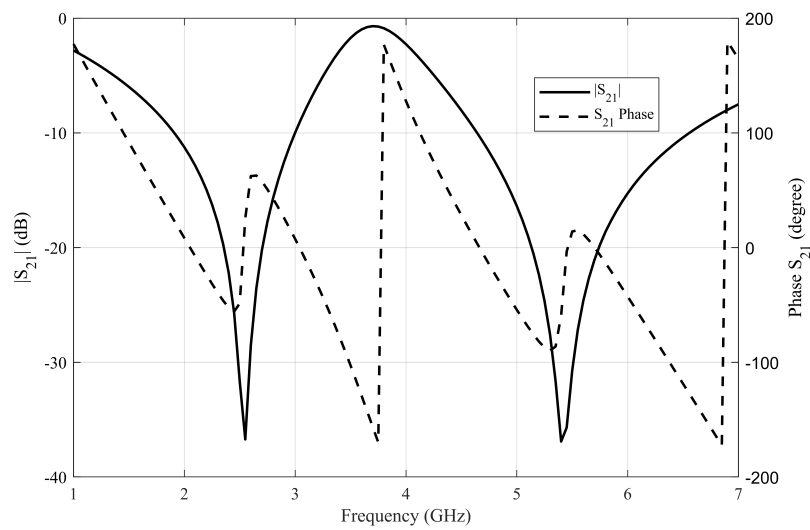


Fig. 7. Amplitude and phase of the optimized FSS frequency response.

TABLE II. FINAL DIMENSIONS OF THE DESIGNED FSS.

Parameter	Dimension (mm)
L_{out}	18.3
L_{in}	12.6
W_{out}	1.5
W_{in}	1.0
P	19.3
h	1.6

B. Antenna with FSS Analysis

The dual band monopole antenna is designed to work in the frequency bands of two widely used segments: ISM, operating from 2.4 GHz to 2.4835 GHz and IEEE 802.11, operating from 5.15 GHz to 5.725 GHz. To meet the frequency band requirements, the antenna geometry definition was based on the work of Panda et al [29], which presents a dual-band antenna applied to RFID and WLAN. The proposed structure is shown in Fig. 8.

The 9-shaped microstrip monopole antenna consists of a square loop with a slot, which generates

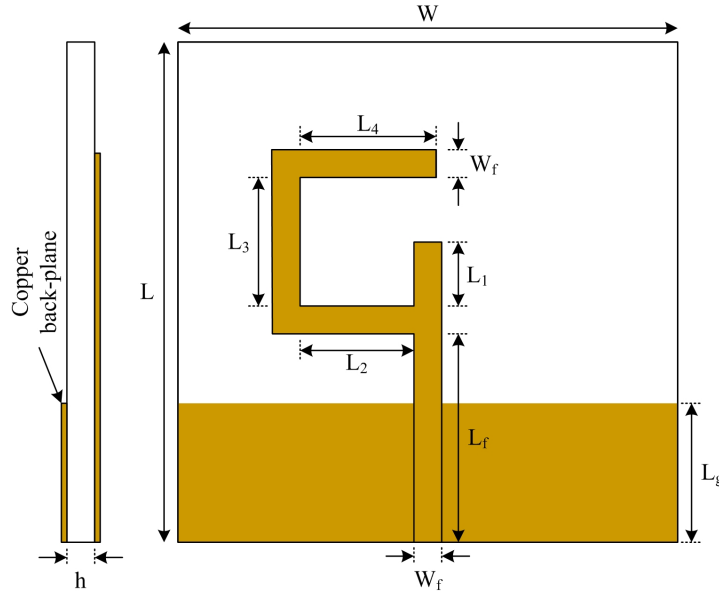


Fig. 8. Proposed antenna and its physical dimensions.

the two resonances in the bands of interest. In addition, the antenna is fed with a 50-ohm microstrip line and has a truncated ground plane. For the chosen monopole antenna, the resonant frequency can be approximately calculated by equating its area to that of an equivalent cylindrical monopole antenna [29] of equivalent height L_c and equivalent radius r_c . The first resonance frequency f_1 (in GHz) of the printed monopole antenna is chosen to be 2.50 GHz and it is calculated as:

$$f_1 = \frac{7.2}{L_c + r_c + p_c} \quad (1)$$

where

$$L_c = L_2 + L_3 + L_4 + 2W_f \quad (2)$$

$$r_c = \frac{W_f(L_1 + L_2 + L_3 + L_4 + 4W_f)}{2\pi(L_2 + L_3 + L_4 + 2W_f)} \quad (3)$$

$$p_c = L_f - L_g \quad (4)$$

The second resonant frequency f_2 is a multiple of the first resonant frequency. Without the element of length L_1 , the radiating element is found to be giving the second resonant frequency at 5.00 GHz, including this L_1 in the radiating element, the second resonant frequency is obtained at 4.95 GHz. Thus this small length L_1 is shifting the second resonant. By properly varying the dimensions of the antenna, we can fix the antenna resonance at 2.50 GHz and 4.95 GHz, respectively. The 9-shaped microstrip monopole antenna consists of a square loop with a slot, which generates the two resonances in the bands of interest. In addition, the antenna is fed with a 50-ohm microstrip line and has a truncated ground plane. As shown in Fig. 8, the optimized dimensions achieved were (units in millimeters): $L_1 = 1$, $L_2 = 5.4$, $L_3 = 10$, $L_4 = 7$, $L_f = 14$, $W_f = 3.0$ and $L_g = 12$. The antenna uses a low-cost FR-4 substrate with a dielectric constant of 4.4, and a loss tangent of 0.02. The substrate dimensions were:

$W = 30$ mm, $L = 38$ mm and thickness, h , of 1.6 mm.

We designed and incorporated an FSS-based reflector to enhance the antenna performance, composing a new structure with improved radiation parameters that will be described and analyzed in this work. Once the dimensions of the FSS were defined, a 3D model of the surface-integrated antenna was built in the HFSS software with a distance d between the antenna and the projected FSS, which was initially set at 20 mm. With the model created in HFSS, a parametric analysis of d was carried out to find the optimal value for this dimension. The result of this analysis is illustrated in Fig. 9, which shows the S_{11} of the antenna with the integrated FSS, for different values of d .

Analyzing the results presented in Fig. 9, the optimal distance between the FSS and the monopole was 35 mm. This distance between the two structures was considered optimal because the parametric analysis shows that at this distance the antenna with the FSS meets the desired frequency bands (2.13 - 3.00 GHz and 4.44 - 6.54 GHz) and presents a better impedance matching.

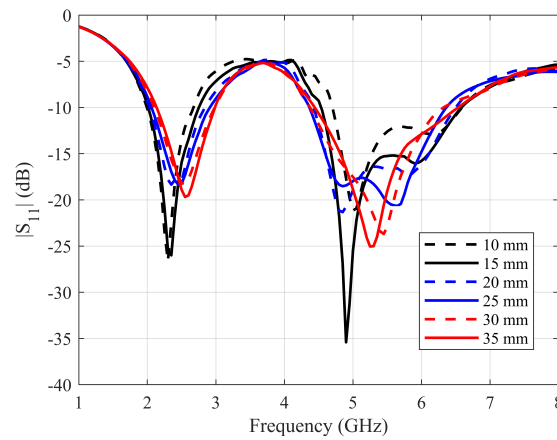


Fig. 9. Parametric analysis of the distance between antenna and FSS

Other important parameters needed to be compared to prove the improvements with the insertion of the FSS as a reflector [30], [31], [32], [33], [34]. So, in Fig. 10, we illustrate the simulated parameters S_{11} , gain, efficiency, and front-to-back ratio (FBR) of the antenna without and with the FSS. We can see in Fig. 10(a), for the antenna, that the resonance frequencies are 2.50 GHz and 4.95 GHz. The S_{11} levels are - 21.35 dB and - 24.87, at 2.50 GHz and 4.95 GHz, respectively. The fractional bandwidths are 28.4% and 44.9%, respectively. For the antenna with the FSS, the resonance frequencies are 2.55 GHz and 5.30 GHz. The S_{11} levels are - 25.01 dB and - 26.65, at 2.55 GHz and 5.30 GHz, respectively. The fractional bandwidths are 34.1% and 39.6%, respectively. There is a small increase in bandwidth in the first operating band and a small decrease in bandwidth in the second operating band, but those bands cover the bands of ISM and UNII applications. In Fig. 10(b) we can see that the gains are - 0.85 dBi and 4.18 dBi, at 2.50 GHz and 4.95 GHz, respectively, for the antenna. For the antenna with the FSS, the gains are 2.26 dBi and 6.62 dBi, at the resonance frequencies. We can observe an increase in the directivity with the integration of the FSS. Fig. 10(c) shows the simulated (with the software HFSS) radiation efficiency of the proposed antenna with and without the FSS; It shows that the antenna with the FSS reflector achieves a maximum radiation efficiency of 95.8% and 94% at the two operating bands. An improvement in efficiency is not noticed (it is the same in the 2.45 GHz band) since the antenna efficiency is already high without the FSS. Fig. 10(d) illustrates this parameter. For the antenna, the FBRs are 1.18 dB and 15.16 dB, at the two operating bands. For the antenna with the

FSS, the FBRs are 11.23 dB and 21.89 dB, at the two operating bands. As we can see, all important parameters are improved with the integration of the FSS. A better comparison of the results can be seen in Table III.

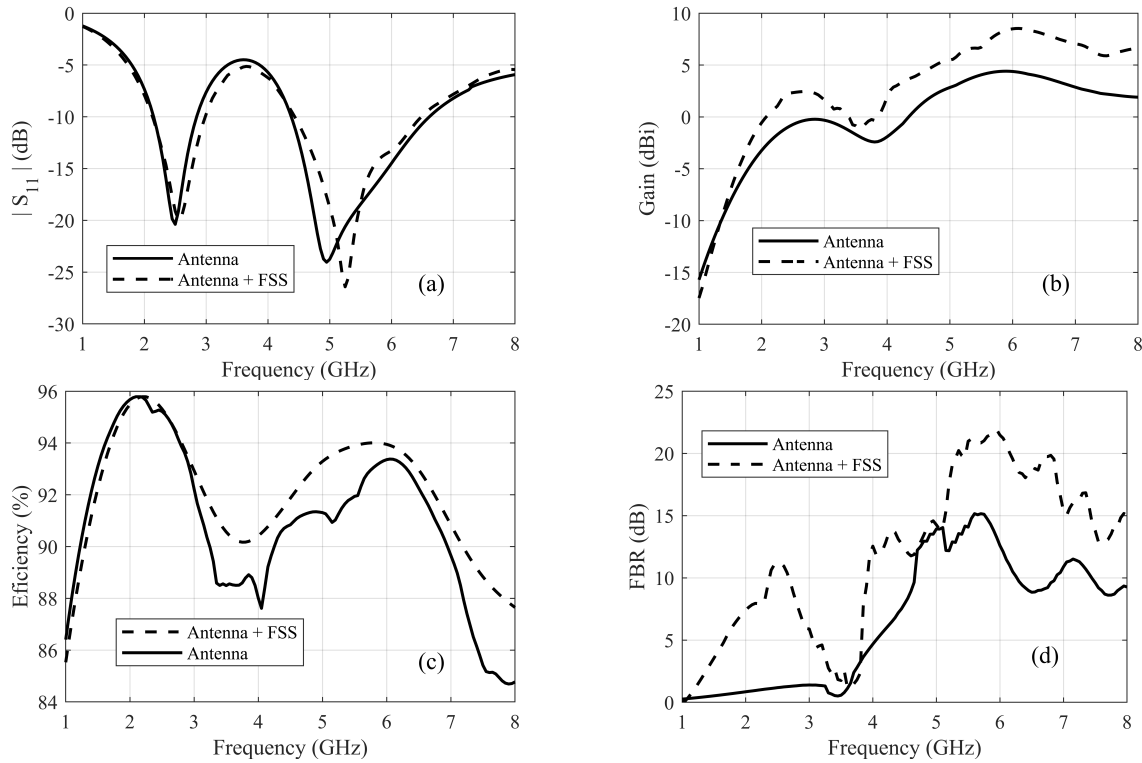


Fig. 10. Parameters of the antenna without and with the integrated FSS: (a) $|S_{11}|$, (b) gain, (c) efficiency, and (d) FBR.

The simulated radiation pattern in the E plane of the proposed antenna without and with FSS at 2.5 GHz and 5 GHz are presented in Fig. 11(a) - Fig. 11(d) and the H plane are presented in Fig. 12(a) - Fig. 12(d). These Figs. depicts the effect of FSS on FBR and gain, but also indicates that the proposed antenna doesn't have polarization purity, because of the horizontal arms of the 9-shaped format. Even without polarization purity, we selected the 9-shaped antenna because of its bandwidth and dual-band frequency response, covering, entirely, the main bands used in biomedical applications (ISM and UNII).

IV. EXPERIMENTAL RESULTS

For validation of the proposed structure, prototypes of both the antenna and the reflector were fabricated using an FR-4 dielectric, assembled, and experimentally characterized. Fig. 13 presents a photo of the fabricated prototype, containing the reflector (Fig. 13(a)), which has a total size of 142 mm x 142 mm x 1.6 mm and with 8 x 8 unit cells and antenna (Fig. 13(b)). The proposed structure was measured at the GTEMA/IFPB microwave laboratory, using the free-space method, as shown in Fig. 14. Furthermore, the setup comprises an Agilent E5071C vector network analyzer and a pair of standard gain horn antennas. The fabricated sample is inserted into a frame surrounded by an absorbent material, which is placed in front of the antennas. To ensure that the sample can receive and reflect signals, both the antenna and sample centers are kept at the same height. In the measurements, the FSS was kept at a distance of 1.7 m from the horn antennas, which ensures that the FSS is positioned in the far-field region and that the incident wave is plane.

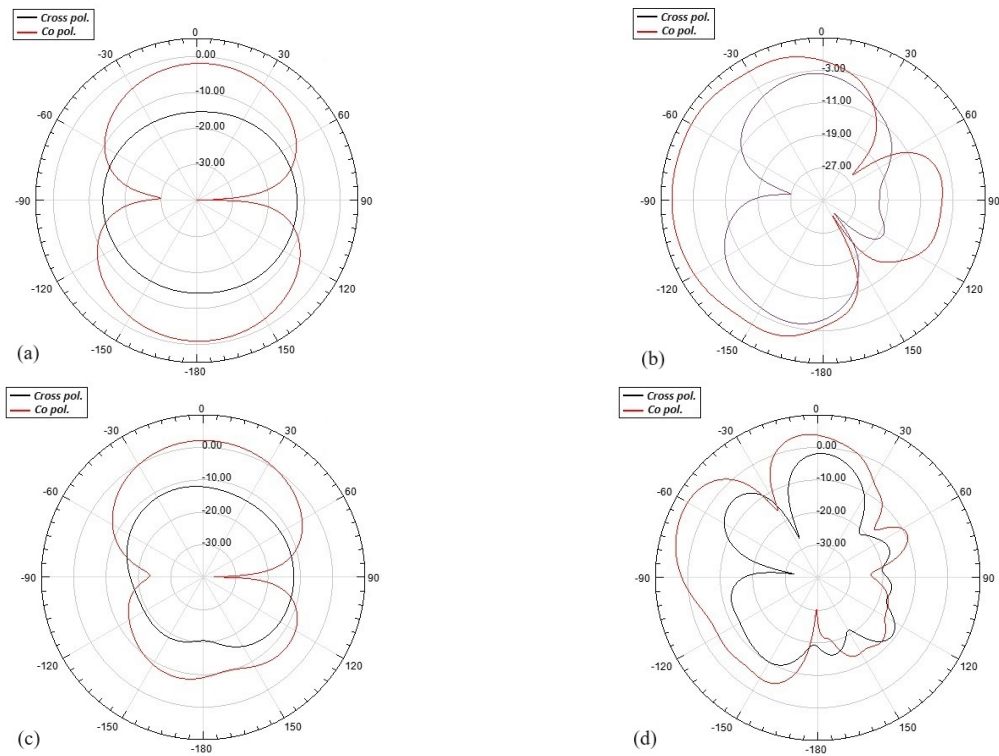


Fig. 11. Simulated radiation pattern in E plane: (a) antenna without FSS at 2.50 GHz, (b) antenna without FSS at 4.95 GHz, (c) antenna with FSS at 2.55 GHz, (d) antenna with FSS at 5.30 GHz.

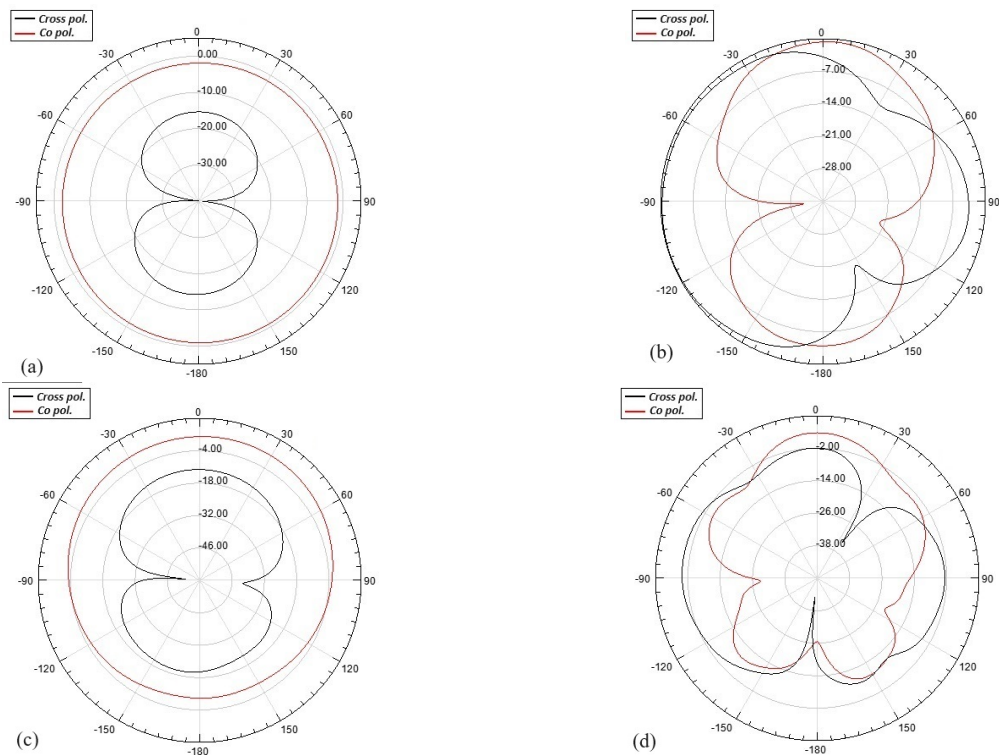


Fig. 12. Simulated radiation pattern in H plane: (a) antenna without FSS at 2.50 GHz, (b) antenna without FSS at 4.95 GHz, (c) antenna with FSS at 2.55 GHz, (d) antenna with FSS at 5.30 GHz.

The experimental and simulated results for the FSS transmission coefficient under normal incidence

TABLE III. COMPARISON BETWEEN SIMULATED RESULTS OBTAINED FROM THE RADIATION CHARACTERISTICS OF THE ANTENNA WITHOUT AND WITH FSS.

Parameter	Structure	
	Antenna	Antenna with FSS
f_R (GHz)	2.50	2.55
	4.95	5.30
$ S_{11} $ level (dB)	- 21.35	- 25.01
	- 24.87	- 26.65
Fractional bandwidth (%)	28.4	34.1
	44.9	39.6
Gain (dBi)	- 0.85	2.26
	4.18	6.62
Efficiency (%)	95.8	95.8
	93.4	94.0
FBR (dB)	1.18	11.23
	15.16	21.89

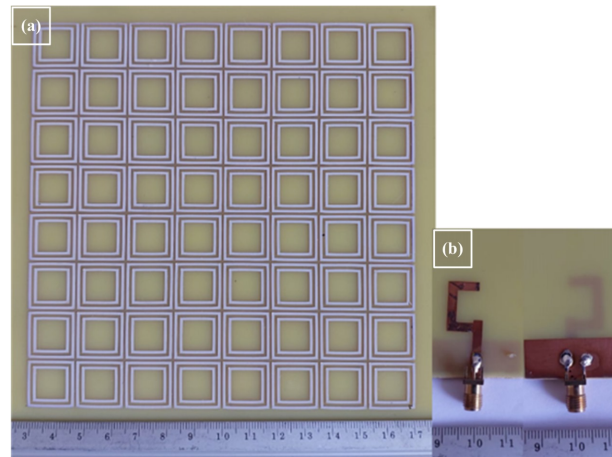


Fig. 13. Photos of the built prototypes: (a) FSS and (b) antenna, front and back.

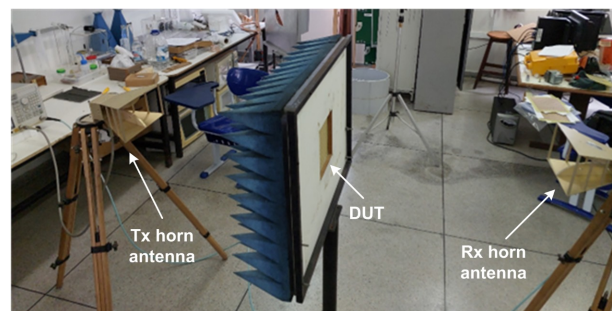


Fig. 14. Measurement setup.

are presented in Fig. 15. The experimental and numerical simulation results show good agreement, in which two rejection bands, the first ranging from 1.9 GHz to 3 GHz (2.40 GHz to 3.10 GHz in measurements) and the second from 4.65 GHz to 6.55 GHz (4.42 GHz to 6.02 GHz in measurements), are shown. As noted, there is a slight divergence in bandwidths between the results. However, the bands of interest are covered by the constructed FSS.

Fig. 16 illustrates a non-normalized version of the results of Fig. 15. This allows the readers to

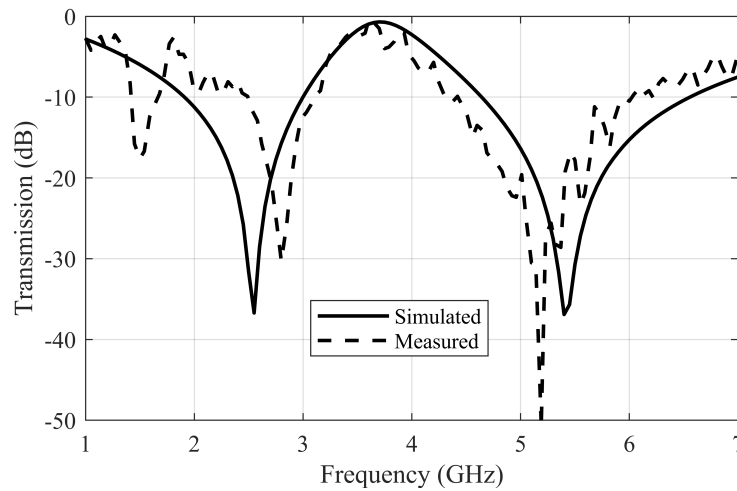


Fig. 15. Comparison between simulated and measured FSS transmission results.

understand how the horn gains, free-space path loss, and connectors' losses are considered to obtain the FSS response. The reference curve is measured without the FSS between the two horn antennas, to get the effect of the measurement environment, antenna gains, connector and cable losses, and free space loss. After this, the FSS response is measured and subtracted from the reference curve, resulting in the normalized curve of the transmission coefficient through the structure, showing how the FSS reflects the two desired bands.

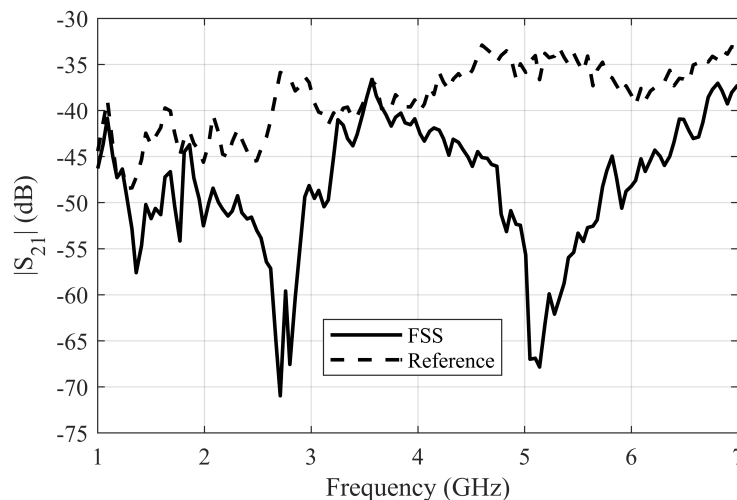


Fig. 16. Non-normalized version of the results of reference and FSS frequency response.

Measurements regarding the angular stability of the designed FSS were also carried out and can be seen in Fig. 17(a) and Fig. 17(b). In it, we can observe the angular stability of the planar filter in both vertical (Fig. 17(a)) and horizontal (Fig. 17(b)) polarization. These measurements show that the designed FSS presents angular stability for incidence angles of up to 40° in both vertical and horizontal polarization. Thus showing even better results than the simulations, which predicted angular stability only for angles of up to 30°.

To investigate the influence of the FSS reflector on the radiation characteristics, integrated structure measurements were performed. Since the reflector was designed to act as a stopband filter, it was inserted behind the antenna so it could reflect the signals in phase. The sample photograph of the integrated

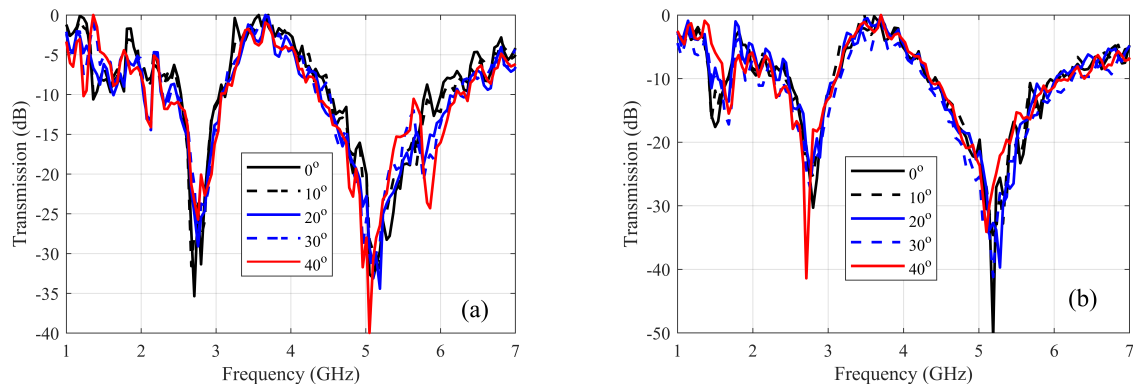


Fig. 17. Angular stability for: (a) vertical polarization and (b) horizontal polarization.

structure is shown in Fig.18. The reflected waves can contribute to the antenna gain. Furthermore, as the device operates in two bands, the optimal distance between the FSS and the antenna had to be determined. The 35 mm distance showed better simulation results in the two bands of interest and was used in the final structure.

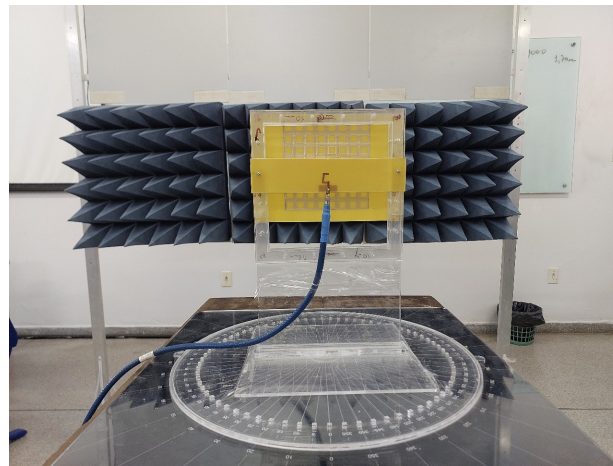


Fig. 18. Integrated prototype of the proposed antenna.

Fig. 19 illustrates a comparison between the measured results of $|S_{11}|$ without and with the integrated FSS. As can be seen, the FSS keeps the operating bands almost intact and improves the impedance matching, achieving almost -20 dB of $|S_{11}|$ level in the lower frequency range, with a bandwidth of 650 MHz (2.35 GHz to 3.00 GHz), and more than -30 dB of $|S_{11}|$ level in the second band and 1.1 GHz bandwidth (4.88 GHz to 5.98 GHz). Fig. 20(a) and Fig. 20(b) compare measured and simulated results for antenna without and with FSS, of $|S_{11}|$. As we can see, a good agreement between the results can be observed.

To compare the radiation properties of the antenna integrated with the FSS reflector, initially, for each frequency (2.55 GHz and 5.30 GHz), the radiation pattern was measured using the two-antenna method and we used one horn antenna and the 9-shaped monopole antenna, without the reflector. Then, the obtained values are normalized concerning their maximum value. After the radiation pattern was measured for the antenna integrated with the FSS reflector the obtained values were normalized to the maximum for the antenna without the FSS. This way, the antenna with and without FSS can be compared. The normalized radiation patterns are shown in Fig. 21(a) and Fig. 21(b). It can be seen that

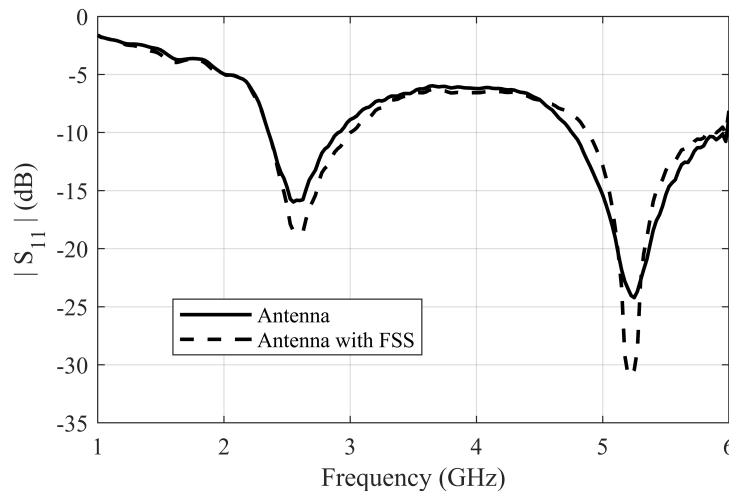


Fig. 19. Comparison between the measured $|S_{11}|$ results for the antenna without and with FSS.

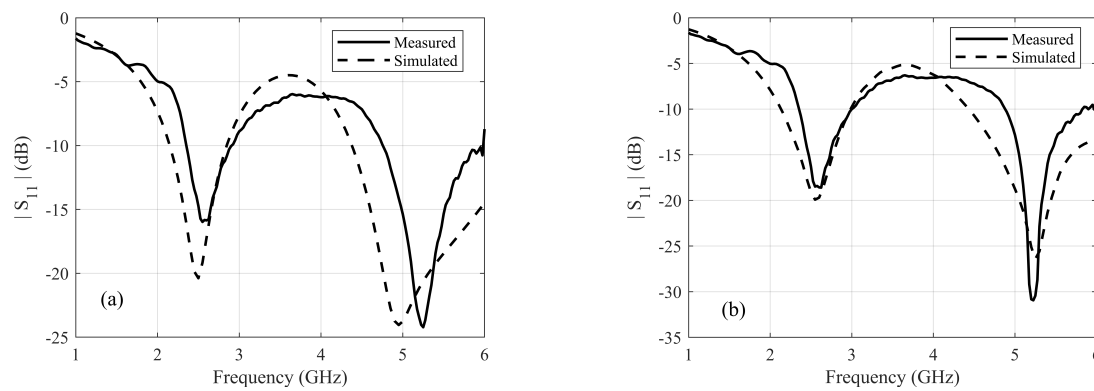


Fig. 20. Comparison between simulated and measured $|S_{11}|$ results for the antenna: (a) without FSS and (b) with FSS.

the integration of the antenna with the FSS modified the radiation characteristics of the antenna, making it more directive, and improving its gain and the front-to-back ratio. More specifically, by analyzing the results obtained, one can observe that the antenna radiation efficiency increased and the back lobes had significant reduction. It is noted that the integration of the FSS provided an increase of 3 dB in the measurements of the antenna gain at the frequency of 2.55 GHz (see Fig. 21(a)) and of 2.6 dB at a frequency of 5.30 GHz (see Fig. 21(b)). Furthermore, increases of 7.5 dB and 4.5 dB were observed in the RFC of the antenna at frequencies of 2.55 and 5.30 GHz, respectively.

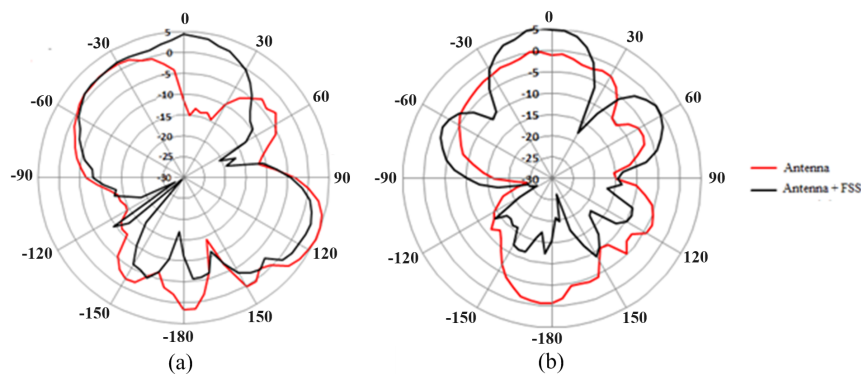


Fig. 21. Radiation patterns for the antenna and the antenna with FSS: (a) 2.55 GHz and (b) 5.30 GHz

Table IV provides a concise comparison between the proposed work and previous related studies. Our proposed antenna demonstrates favorable parameters across all characteristics and exhibits the widest fractional bandwidths compared to prior works featuring dual-band operation. As noted, some antennas have negative gain in dBi. Negative gain values are normal for implantable antennas, as skin tissue is lossy, which causes absorption of part of the wave energy. The comparison of these antennas (references [16] and [23]) with the structure proposed in this work (antenna and FSS), which radiates in free space, was maintained due to the antennas operating in the same frequency range.

TABLE IV. Comparison of the proposed structure with previously presented studies

Ref	Physical Size [mm ³]	Ressonant frequency (GHz)	S ₁₁ level (dB)	Fractional bandwidth (%)	Gain (dBi)	Efficiency (%)	FBR (dB)
[11]	24 × 24 × 0.787	2.34, 3.2, 4.98	- 17.58, - 27.93, - 17.42	18.6, 2.8, 8.5	-	-	-
[14]	50 × 50 × 1.6	2.45, 4.5	- 39, - 30	3.31, 4	3.09, 3.8	-	-
[15]	60 × 60 × 8.72	2.45, 3.45	- 19, - 23	4.9, 6.7	6.8, 9	94, 93	23, 21
[16]	11 × 11 × 0.89	0.915, 2.45	- 13, - 11.5	7.7, 11.3	-28.8, -22.9	-	-
[17]	2.28 × 3.06 × 0.14	33.5, 60.8	-14.8, -12.7	3.5, 1.9	6.02, 7.08	95.7, 96.5	-
[18]	70 × 70 × 1.6	2.4, 5.8, 10.2	-22.5, -43.5, -52.1	5.7, 17.3, 2.7	5.1, 8.2, 13	65.5, 55, 50	20.4, 13.2, 24.4
[19]	30 × 40 × 1	2.4, 9.04	-6.9, 14.9	25.4, 7.4	3.2, 2.8	94, 92.3	-
[20]	85 × 85 × 4	7.02, 9.3	- 47, - 50.2	28.6, 5.4	9.08, 8.49	-	15
[21]	50 × 50 × 0.254	2.4, 3.8, 5.8	-42, -35.8, -24	16, 10.5, 5.21	2.62, 3.95, 4.27	-	-
[22]	25 × 27 × 0.13	5-6	-	-	3.8	98	-
[23]	6 × 6 × 0.25	0.915, 2.4	-	12.6, 12.8	-21, -19	-	-
[24]	80 × 80 × 2	2.4, 5.8	-17.2, -15.4	-	5.14, 7.14	-	-
[25]	90 × 90 × 70	2.56	-37	-	-	-	-
[26]	59 × 55 × 0.1	2.45	-43	45	6.58	98.5	8.4
[27]	60 × 60 × 50	1-6	-12	142	-	80	-
This work	142 × 142 × 38.2	2.4, 5.5	-25.01, -26.65	34.1, 39.6	2.26, 6.2	95.8, 94	11.23, 21.89

V. CONCLUSION

In this work, the project of an FSS designed to operate at ISM (2.4 to 2.5 GHz) and UNII (5.15 to 5.85 GHz) bands was presented. The structure was designed to be integrated with a microstrip antenna, to improve its radiation characteristics to make it suitable for remote patient monitoring systems. In this way, the FSS was designed using the geometry of double square loops, because this geometry presents a double-band response, good angular stability, and polarization independence. The dielectric substrate used in this project was FR4 with a thickness of 1.6 mm. The simulations showed that the designed FSS covers the entire band from 1.91 to 3 GHz and 4.64 to 6.56 GHz. The FSS also presented good angular stability in both operating bands, for incidence angles of up to 40°, in both vertical and horizontal polarization. Then, the designed FSS was integrated with a microstrip antenna and simulated using the commercial HFSS software, to determine whether there was an improvement in some antenna radiation characteristics such as bandwidth, gain, efficiency, and front-to-back ratio (FBR). To achieve this, the integrated antenna was simulated with an FSS mounted as a 4x4 matrix of unit cells at a distance of 35 mm from the antenna. Simulations showed that the FSS-based reflector changed the antenna radiation diagram from omnidirectional to directional, improving important radiation parameters such as input reflection coefficient level, gain, and front-to-back ratio, while maintaining almost intact operating bandwidths and efficiency. Furthermore, the simulated results showed that integrating the FSS changed the antenna radiation diagram from omnidirectional to directional at the two simulated frequencies, 2.55 GHz and 5.30 GHz. Thus, the simulated results show that the integration of the FSS to the microstrip monopole modified its radiation characteristics, making it suitable for remote patient monitoring systems. Finally, a prototype of the designed FSS and another of the chosen planar antenna were manufactured and their parameters were measured and compared to the simulated results.

Measurements of S_{11} of the antenna with and without the FSS, S_{21} of the FSS, and radiation pattern of the antenna with and without the FSS were carried out. The results showed good agreement with the simulated results. Measured and simulated results showed that the FSS changed the antenna radiation diagram from omnidirectional to directional.

ACKNOWLEDGMENT

The authors would like to thank CNPq (303191/2021-0) and UFRN for the funding that made this research possible.

REFERENCES

- [1] Y. Ha, J. i. Jung, Lee, and S. Pyo, "Extremely low-profile monopolar microstrip antenna with wide bandwidth," *Sensors*, vol. 21, no. 16, p. 1–11, 2021, <https://doi.org/10.3390/s21165295>.
- [2] C. A. Balanis, *Antenna theory: analysis and design*. Wiley, 2015.
- [3] P. Parthiban, B.-C. Seet, and X. J. Li, "An ultra-rugged UHF RFID reader antenna: A new design for convention center loading docks [wireless corner]," *IEEE Antennas and Propagation Magazine*, vol. 62, no. 1, pp. 84–95, 2020, <https://doi.org/10.1109/MAP.2019.2946560>.
- [4] S. Shen, C.-Y. Chiu, and R. D. Murch, "A dual-port triple-band l-probe microstrip patch rectenna for ambient RF energy harvesting," *IEEE Antennas and Wireless Propagation Letters*, vol. 16, pp. 3071–3074, 2017, <https://doi.org/10.1109/LAWP.2017.2761397>.
- [5] K. N. Ketavath, D. Gopi, and S. Sandhya Rani, "In-vitro test of miniaturized CPW-fed implantable conformal patch antenna at ISM band for biomedical applications," *IEEE Access*, vol. 7, pp. 43 547–43 554, 2019, <https://doi.org/10.1109/ACCESS.2019.2905661>.
- [6] N. Ganeshwaran, J. K. Jeyaprakash, M. G. N. Alsath, and V. Sathyanarayanan, "Design of a dual-band circular implantable antenna for biomedical applications," *IEEE Antennas and Wireless Propagation Letters*, vol. 19, no. 1, pp. 119–123, 2020, <https://doi.org/10.1109/LAWP.2019.2955140>.
- [7] A. J. A. Al-Gburi, I. B. M. Ibrahim, M. Y. Zeain, and Z. Zakaria, "Compact size and high gain of CPW-fed UWB strawberry artistic shaped printed monopole antennas using FSS single layer reflector," *IEEE Access*, vol. 8, pp. 92 697–92 707, 2020, <https://doi.org/10.1109/ACCESS.2020.2995069>.
- [8] S. R. Thummalluru, R. Kumar, and R. K. Chaudhary, "Isolation enhancement and radar cross section reduction of mimo antenna with frequency selective surface," *IEEE Transactions on Antennas and Propagation*, vol. 66, no. 3, pp. 1595–1600, 2018, <https://doi.org/10.1109/TAP.2018.2794417>.
- [9] R. C. O. Moreira, "Planar antennas integrated with fss for applications in wireless communications systems (in portuguese)," Ph.D. dissertation, Federal University of Rio Grande do Norte, 2012.
- [10] S. Chakraborty, A. J. Islam, M. Mehedi Farhad, M. Mahmudul Hasan, M. Siddat Bin Nesar, and M. A. Rahaman, "Performance studies of uwb microstrip antenna for multipurpose biotelemetry applications," in *2018 International Conference on Innovations in Science, Engineering and Technology (ICISSET)*, pp. 322–327, 2018, <https://doi.org/10.1109/ICISSET.2018.8745572>.
- [11] K. H. Yeap, E. M. F. Tan, T. Hiraguri, K. C. Lai, and K. Hirasawa, "A multi-band planar antenna for biomedical applications," *Frequenz*, vol. 75, no. 5, pp. 221–228, 2021, <https://doi.org/10.1515/freq-2020-0079>.
- [12] R. Del-Rio-Ruiz, J.-M. Lopez-Garde, and J. Legarda, "Planar textile off-body communication antennas: A survey," *Electronics*, vol. 8, no. 6, pp. 714–728, 2019, <https://doi.org/10.3390/electronics8060714>.
- [13] E. F. Freitas, "Parametric analysis of microstrip meander line antennas (mmla) (in portuguese)," Ph.D. dissertation, Federal University Rural do Semi-árido, 2019.
- [14] M. B. Hossain and M. F. Hossain, "A dual band microstrip patch antenna with metamaterial superstrate for biomedical applications," in *2021 International Conference on Electronics, Communications and Information Technology (ICECIT)*, pp. 1–4, 2021, <https://doi.org/10.1109/ICECIT54077.2021.9641174>.
- [15] T. T. Le and T.-Y. Yun, "Wearable dual-band high-gain low-sar antenna for off-body communication," *IEEE Antennas and Wireless Propagation Letters*, vol. 20, no. 7, pp. 1175–1179, 2021, <https://doi.org/10.1109/LAWP.2021.3074641>.
- [16] J. Hong, Y. Fan, and X. Liu, "Dual-mode implantable antenna with dual bands for omnidirectionally in-body and circularly polarized off-body communications," in *2022 IEEE MTT-S International Microwave Biomedical Conference (IMBioC)*, pp. 102–104, 2022, <https://doi.org/10.1109/IMBioC52515.2022.9790282>.

- [17] U. Farooq and G. M. Rather, "A miniaturised Ka/V dual band millimeter wave antenna for 5G body centric network applications," *Alexandria Engineering Journal*, vol. 61, no. 10, pp. 8089–8096, 2022, <https://doi.org/10.1016/j.aej.2022.01.044>.
- [18] M. N. Mohanty and S. Mahapatra, "Multiband hexagonal patch antenna for high data rate wearable applications," *Iranian Journal of Science and Technology, Transactions of Electrical Engineering*, vol. 46, no. 4, pp. 925–934, 2022, <https://doi.org/10.1007/s40998-022-00516-2>.
- [19] M. K. Mulaparti, U. V. Ratnakumari, and M. Satyannarayana, "On body and off-body performance analysis of an ashoka tree shaped wearable textile antenna for biomedical and military applications," *Radio Science*, vol. 58, no. 5, pp. 1–13, 2023, <https://doi.org/10.1029/2022RS007626>.
- [20] H. A. Muhammad, Y. I. Abdulkarim, P. A. Abdoul, and J. Dong, "Textile and metasurface integrated wide-band wearable antenna for wireless body area network applications," *AEU - International Journal of Electronics and Communications*, vol. 169, pp. 154 759–154 770, 2023, <https://doi.org/10.1016/j.aeue.2023.154759>.
- [21] S. Prakash, K. Kumar, M. Arulaalan, and M. Kalaivanan, "A hybrid cubic dielectric loaded tri-band antenna for biomedical applications," in *2023 2nd International Conference on Smart Technologies and Systems for Next Generation Computing (ICSTSN)*, pp. 1–5, 2023, note = <https://doi.org/10.1109/ICSTSN57873.2023.10151556>.
- [22] M. E. Yassin, K. F. A. Hussein, Q. H. Abbasi, M. A. Imran, and S. A. Mohassieb, "Flexible antenna with circular/linear polarization for wideband biomedical wireless communication," *Sensors*, vol. 23, no. 12, pp. 5608–5633, 2023, <https://doi.org/10.3390/s23125608>.
- [23] A. Lamkaddem, A. E. Yousfi, V. González-Posadas, and D. Segovia-Vargas, "Miniaturized dual band implantable antenna for implanted biomedical devices," *IEEE Access*, vol. 12, pp. 15 026–15 036, 2024, <https://doi.org/10.1109/ACCESS.2024.3357488>.
- [24] R. Sreemathy, S. Hake, S. V. Gaikwad, S. K. Saw, and S. Behera, "Design, analysis and fabrication of dual frequency distinct bandwidth slot loaded wash cotton flexible textile antenna for ism band applications," *Progress In Electromagnetics Research M*, vol. 109, pp. 191–203, 2022, <https://doi.org/10.2528/PIERM22011203>.
- [25] D. Brizi, M. Conte, and A. Monorchio, "A performance-enhanced antenna for microwave biomedical applications by using metasurfaces," *IEEE Transactions on Antennas and Propagation*, vol. 71, no. 4, pp. 3314–3323, 2023, <http://dx.doi.org/10.1109/TAP.2023.3242414>.
- [26] M. E. Atrash, O. F. Abdalgalil, I. S. Mahmoud, M. A. Abdalla, and S. R. Zahran, "Wearable high gain low SAR antenna loaded with backed all-textile EBG for wban applications," *IET Microwaves, Antennas & Propagation*, vol. 14, pp. 791–799, 2020, <http://dx.doi.org/10.1049/iet-map.2019.1089>.
- [27] O. F. et al., "UWB bowtie antenna for medical microwave imaging applications," *IEEE Transactions on Antennas and Propagation*, vol. 70, no. 7, pp. 5357–5372, 2022, <https://doi.org/10.1109/TAP.2022.3161355>.
- [28] B. A. Munk, *Frequency selective surfaces: theory and design*. Willey, 2005.
- [29] J. R. Panda, A. S. R. Saladi, and R. S. Kshetrimayum, "A compact printed monopole antenna for dual-band RFID and WLAN applications," *Radioengineering*, vol. 20, no. 2, pp. 464–467, 2011.
- [30] S. Mukherjee, A. Roy, A. Mukherjee, S. Kundu, P. Pratim Sarkar, and S. Bhunia, "Notch band characteristics improvement of a printed ultra wideband antenna by embedding frequency selective surface," *AEU - International Journal of Electronics and Communications*, vol. 178, pp. 155 276–155 278, 2024, <https://doi.org/10.1016/j.aeue.2024.155276>.
- [31] S. Maity, T. Tewary, S. Mukherjee, A. Roy, P. P. Sarkar, and S. Bhunia, "Wideband hybrid microstrip patch antenna and gain improvement using frequency selective surface," *International Journal of Communication Systems*, vol. 35, no. 14, pp. e5268–e5291, 2022, <https://doi.org/10.1002/dac.5268>.
- [32] T. Tewary, S. Maity, A. Roy, and S. Bhunia, "Wide band microstrip patch antenna with enhanced gain using fss structure," *Journal of Microwaves, Optoelectronics and Electromagnetic Applications*, vol. 22, no. 2, pp. 329–345, 2023, <https://doi.org/10.1590/217910742023v22i2273333>.
- [33] T. Tewary, S. Maity, S. Mukherjee, A. Roy, P. Sarkar, and S. Bhunia, "FSS embedded high gain 'n' shaped miniaturized broadband antenna," *AEU - International Journal of Electronics and Communications*, vol. 158, pp. 154 465–154 488, 2023, <https://doi.org/10.1016/j.aeue.2022.154465>.
- [34] T. Tewary, S. Maity, A. Roy, K. Mandal, S. Kundu, and S. Bhunia, "Design and analysis of frequency selective surface embedded broadband high gain miniaturized antenna," *International Journal of Communication Systems*, vol. 37, no. 8, pp. e5754–e5773, 2024, <https://doi.org/10.1002/dac.5754>.